

# Effects of a magnetic field on vortex states in superfluid $^3\text{He-B}$

Kenichi Kasamatsu<sup>1</sup>, Ryota Mizuno<sup>2</sup>, Tetsuo Ohmi<sup>1</sup>, and Mikio Nakahara<sup>3,4</sup>

<sup>1</sup>*Department of Physics, Kindai University, Higashi-Osaka, Osaka 577-8502, Japan*

<sup>2</sup>*Department of Physics, Osaka University, 1-1 Machikaneyama-cho, Toyonaka, Osaka, 560-0043, Japan*

<sup>3</sup>*Department of Mathematics, Shanghai University, 99 Shangda Road, Shanghai 200444, China and*

<sup>4</sup>*Research Institute for Science and Technology, Kindai University, Higashi-Osaka, 577-8502, Japan*

(Dated: March 22, 2021)

Superfluid  $^3\text{He-B}$  possesses three locally stable vortices known as a normal-core vortex ( $o$ -vortex), an A-phase-core vortex ( $v$ -vortex), and a double-core vortex ( $d$ -vortex). In this work, we study the effects of a magnetic field parallel or perpendicular to the vortex axis on these structures by solving the two-dimensional Ginzburg-Landau equation for two different sets of strong coupling correction. The energies of the  $v$ - and  $d$ -vortices have nontrivial dependence on the magnetic field. As a longitudinal magnetic field increases, the  $v$ -vortex is energetically unstable even for high pressures and the  $d$ -vortex becomes energetically most stable for all possible range of pressure. For a transverse magnetic field the energy of the  $v$ -vortex becomes lower than that of the  $d$ -vortex in the high pressure side. In addition, the orientation of the double cores in the  $d$ -vortex prefers to be parallel to the magnetic field at low pressures, while the  $d$ -vortex with the double cores perpendicular to the magnetic field is allowed to continuously deform into the  $v$ -vortex by increasing the pressure.

PACS numbers: 67.30.he

## I. INTRODUCTION

Superfluid  $^3\text{He}$  is a typical anisotropic Fermionic superfluid consisting of spin-triplet  $p$ -wave Cooper pairs.<sup>1</sup> The order parameter of superfluid  $^3\text{He}$  is characterized by  $3 \times 3$  complex fields, which allows an existence of a rich variety of topological excitations. An example of topological excitations is a quantized vortex. Quantized vortices in superfluid  $^3\text{He}$  involve extremely rich physical phenomena and this topic has been studied for decades.<sup>2,3</sup>

Quantized vortices in superfluid  $^3\text{He}$  are classified by the symmetry property.<sup>4,5</sup> Several types of axisymmetric vortices exist, depending on which discrete symmetries are preserved in the order parameter of the vortex states. The actual vortex structure at given temperature and pressure is obtained by minimizing the appropriate free energy. For the  $^3\text{He-B}$  phase, from many theoretical studies, it has been known that three types of vortices exist as the local minima of the free energy. One possible structure is known as the  $o$ -vortex,<sup>6,7</sup> which preserves the maximal symmetry group and its core is filled with the normal component. However, the  $o$ -vortex is not the absolute energy minimum state in the parameter region where the B phase is stable.<sup>4,8</sup> Another axisymmetric vortex is the  $v$ -vortex,<sup>4,8</sup> which has magnetic reflection symmetry on a plane including the vortex line. The core of the  $v$ -vortex is filled with the A-phase and the  $\beta$ -phase components. In experiments, the  $v$ -vortex exists in high-temperature and high-pressure region in the  $p$ - $T$  phase diagram of superfluid  $^3\text{He-B}$ .<sup>9</sup> For low-temperature and low-pressure region, however, the axisymmetry of the  $v$ -vortex is spontaneously broken into the double vortex-core structure, known as the  $d$ -vortex. Thuneberg revealed this double-core structure by direct numerical minimization of the Ginzburg-Landau (GL) free energy functional.<sup>10,11</sup> The  $d$ -vortex can be interpreted as two half-quantum vortices

bound together by the planar phase.<sup>10-12</sup> The nonaxisymmetric feature of the  $d$ -vortex has been experimentally observed by Kondo *et al.*<sup>13</sup> through the measurement of a new Goldstone mode associated with the spiral twisting of the anisotropic core. The vortex core structure has been also calculated based on the quasiclassical Eilenberger equation.<sup>14-16</sup> This method is applicable to the weak-coupling regime, although it cannot explain the pressure dependence of the vortex structure in the strong-coupling regime.

The purpose of this paper is to analyze the influence of a magnetic field on the stability of the aforementioned vortices. We calculate the energy of the vortices using the GL free energy, and construct the phase diagram of vortices in the pressure and magnetic-field-strength plane. Here, the effect of a magnetic field is included through the quadratic term in the GL free energy. The energetic stability is nontrivial because the magnetic field suppresses some order parameter components in the core of the  $v$ - and  $d$ -vortices. To obtain the reliable results of the vortex energy, it is important to use the newly-proposed values of the strong coupling correction for the  $\beta$ -parameters in the bulk GL free energy.<sup>17</sup> To this end, we adapt two different data sets. One is the Sauls-Serene values (Set I),<sup>18</sup> which was employed in the seminal paper by Thuneberg.<sup>10,11</sup> The other is obtained by optimizing various experimental data<sup>19</sup> (Set II). We find that, although both parameter sets give qualitatively similar vortex phase diagrams without a magnetic field, the Set II provides it closer to the experimental observations. When a magnetic field parallel to the vortex axis is turned on within the range where the bulk B-phase is thermodynamically stable, the  $d$ -vortex is the most stable structure throughout the pressure range. A magnetic field perpendicular to the vortex axis stabilizes the  $v$ -vortex; as the field strength increases, the stable region of the  $v$ -vortex extends to the lower pressure region. It

also breaks the rotational degeneracy with respect to the symmetry axis of the  $d$ -vortex.

This paper is organized as follows. In Sec. II A, we outline the GL free energy required to analyze the vortex structure in superfluid  $^3\text{He-B}$  and list two sets of parameters in the energy functional. Section II B briefly reviews the bulk energy of superfluid  $^3\text{He}$  and Sec. II C describes the prescription of the numerical calculation. In Sec. II D, we show the numerical results for the case without the magnetic field, which is compared with those of the previous literature to confirm the validity of our calculation. Section III is the main part of our paper, where we show the numerical analysis of vortices in the presence of a magnetic field parallel (Sec. III A) and perpendicular (Sec. III B) to the vortex axis. Section IV is devoted to conclusion.

## II. GINZBURG-LANDAU THEORY OF VORTEX STATES IN SUPERFLUID $^3\text{He}$

We first introduce a formulation based on the GL free energy functional for the order parameter of superfluid  $^3\text{He}$ . After describing the numerical procedure of the energy minimization, we analyze vortices in the B-phase without a magnetic field and compare the results with those of the previous work to justify our calculation. We repeat the calculation with the parameters Set I and Set II for the strong coupling corrections and reproduce the results in Thuneberg<sup>10,11</sup> for Set I. The results for Set II have not been reported before.

### A. Ginzburg-Landau Free Energy

The order parameter of superfluid  $^3\text{He}$  is given by a gap function  $\hat{\Delta}$ , which is a symmetric  $2 \times 2$  matrix in spin space.<sup>1,2</sup> By introducing the  $\mathbf{d}$ -vector  $\mathbf{d} = (d_x, d_y, d_z)$ , the gap function can be written as  $\hat{\Delta} = id_\mu \sigma_\mu \sigma_y$ , where  $\sigma = (\sigma_x, \sigma_y, \sigma_z)$  is the Pauli matrix and summation over repeated indices is understood. By incorporating the representation  $d_\mu = A_{\mu i} \hat{p}_i$  with unit vector  $\hat{\mathbf{p}} = (\hat{p}_x, \hat{p}_y, \hat{p}_z)$  of the momentum on the Fermi surface, we write

$$\hat{\Delta}(\hat{\mathbf{p}}) = iA_{\mu i} \sigma_\mu \sigma_y \hat{p}_i, \quad (\mu, i = x, y, z). \quad (1)$$

Thus, superfluid  $^3\text{He}$  is characterized by complex tensor  $(A_{\mu i})$  inherent in the  $p$ -wave ( $L = 1$ ) and spin-triplet ( $S = 1$ ) pairing, where  $\mu$  and  $i$  refer to the spin and the orbital indices, respectively.

The GL theory is valid when we confine ourselves within the situation near the superfluid transition temperature  $T \lesssim T_c$ . By using  $A_{\mu i}$ , the bulk free energy density in the GL expansion takes the form

$$\begin{aligned} f_B = & -\alpha(t) A_{\mu i}^* A_{\mu i} + \beta_1 A_{\mu i}^* A_{\mu i}^* A_{\nu j} A_{\nu j} \\ & + \beta_2 A_{\mu i}^* A_{\mu i} A_{\nu j}^* A_{\nu j} + \beta_3 A_{\mu i}^* A_{\nu i}^* A_{\mu j} A_{\nu j} \\ & + \beta_4 A_{\mu i}^* A_{\nu i} A_{\nu j}^* A_{\mu j} + \beta_5 A_{\mu i}^* A_{\nu i} A_{\nu j} A_{\mu j}^*, \end{aligned} \quad (2)$$

which is invariant under separate spin and real space rotations in addition to the gauge transformation, namely  $U(1) \times SO^{(S)}(3) \times SO^{(L)}(3)$ . The coefficient  $\alpha(t)$  of the second order term has a temperature dependence  $\alpha(t) = \alpha_0 t$  with a constant  $\alpha_0$  and a small parameter  $t = 1 - T/T_c$ .

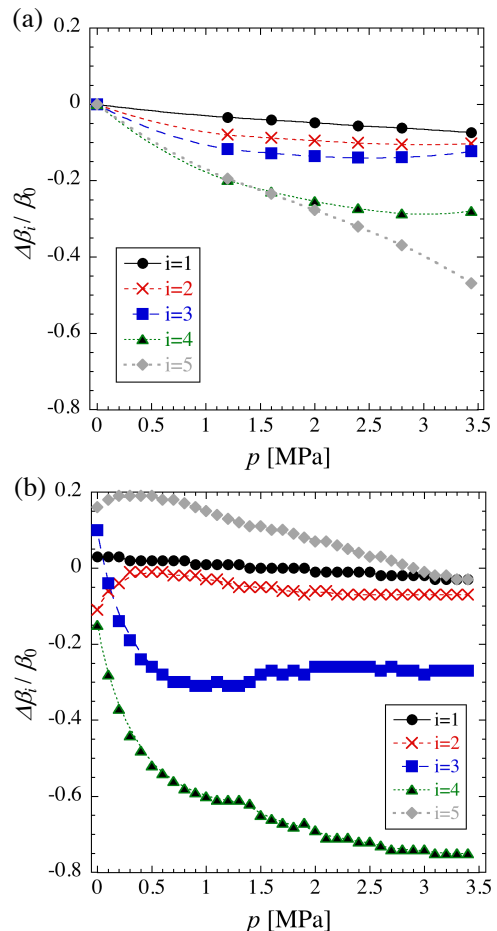


FIG. 1. (Color online) Strong coupling correction  $\Delta\beta_i$  ( $i=1-5$ ). The data points are taken from Ref.<sup>18</sup> [Set I] (a) and Ref.<sup>19</sup> [Set II] (b), and the curves represent the interpolating functions.

We consider the pressure range  $0 \leq p \leq 3.44$  MPa, beyond which the system solidifies. The fourth order contribution to the bulk free energy has five terms with coefficients  $\beta_j$ . In the weak-coupling limit at zero pressure, these coefficients satisfy the relation

$$-2\beta_1^{\text{wc}} = \beta_2^{\text{wc}} = \beta_3^{\text{wc}} = \beta_4^{\text{wc}} = -\beta_5^{\text{wc}} \equiv 2\beta_0, \quad (3)$$

where  $\beta_0 = 7\zeta(3)N(0)/[120\pi^2(k_B T_c)^2]$  with the density of states at the Fermi surface per spin  $N(0)$  and the Riemann zeta function  $\zeta(3)$ . The pressure dependence can be included by the strong-coupling corrections for  $\beta_j$ , which are written as  $\Delta\tilde{\beta}_j = \Delta\beta_j/\beta_0 = (\beta_j - \beta_j^{\text{wc}})/\beta_0$ . However, the exact values of the correction as functions of the pressure have not been known. Here, we use two data sets. One is the theoretical evaluation by Sauls and

TABLE I. List of the coefficients for the fitting of the correction of  $\beta$  according to the paper by Sauls and Serene.<sup>18</sup> Write “Set I”.

$j$	$A_j^{(1)}$	$A_j^{(2)}$	$A_j^{(3)}$	$A_j^{(4)}$
1	-0.041318	0.015586	-0.0043854	0.00044482
2	-0.13306	0.081867	-0.025704	0.0030876
3	-0.18713	0.10679	-0.030986	0.0037026
4	-0.28746	0.14638	-0.043984	0.0054785
5	-0.24049	0.090797	-0.023003	0.0015738

Serene.<sup>18</sup> In their paper, the values of  $\Delta\tilde{\beta}_j$  for six values of pressure are given. In our work, these points and  $\Delta\tilde{\beta}_j = 0$  at  $p = 0$ , where  $\beta_j(p = 0)$  coincide with the weak-coupling values of Eq. (3), are interpolated through the 4-th order polynomials  $\Delta\tilde{\beta}_j = \sum_{k=1}^4 A_j^{(k)} p^k$  as shown in Fig. 1 (a), where  $p$  [MPa] is pressure. The list of the fitting parameters  $A_j^{(k)}$  are shown in Table I. We refer to this set of  $\beta_j$  as “Set I”.

The other is described in Choi *et al.*,<sup>19</sup> which reports a new data of the  $\beta_i$ -values as functions of the pressure based on past experiments. The thermodynamic properties of superfluid <sup>3</sup>He have been better accounted for by the analysis with this new  $\beta_j$ -values.<sup>20</sup> We also use the values of  $\beta_j$  following Ref.<sup>19</sup>; numerical fitting of the data with the 9-th order polynomials  $\Delta\tilde{\beta}_j = \sum_{k=0}^9 B_j^{(k)} p^k$  is shown in Fig. 1 (b), where the coefficients  $B_j^{(k)}$  are listed in Table II. We refer to this set of  $\beta_j$  as “Set II”. The obvious differences between Figs. 1(a) and 1(b) are that the values of  $\beta_i$  at  $p = 0$  are slightly shifted from the weak-coupling values, and the magnitude of the correction is relatively large for  $\beta_3$  and  $\beta_4$  in Fig. 1(b); especially  $\Delta\beta_5$  gives a positive correction in contrast with the Set I case. This parameter set energetically favors the emergence of the A-phase component in the bulk phase diagram compared to the case of Set I, as seen in Ref.<sup>20</sup> and discussed below.

The gradient energy in the GL expansion is given by

$$f_G = K_1 \partial_i A_{\mu j} \partial_i A_{\mu j}^* + K_2 \partial_i A_{\mu i} \partial_j A_{\mu j}^* + K_3 \partial_i A_{\mu j} \partial_j A_{\mu i}^*. \quad (4)$$

The coefficients  $K_i$  satisfy  $K_1 = K_2 = K_3 = K$  in the weak-coupling limit, which we employ in the rest of this paper for simplicity. By comparing the gradient term and the first term of the bulk energy [Eq. (2)], the coherence length is defined as

$$\xi(t) = \sqrt{\frac{K}{\alpha(t)}} = \sqrt{\frac{K}{\alpha_0}} \frac{1}{\sqrt{t}}. \quad (5)$$

The minimum length scale of our problem is the coherence length at zero temperature  $\xi(0) = \sqrt{K/\alpha_0} \sim 0.01 \mu\text{m}$ .

In this work, we consider the effect of a magnetic field on the vortex state. We take account of this ef-

fect through the second order magnetic free energy given by

$$f_M = g_m H_\mu A_{\mu i}^* H_\nu A_{\nu i}, \quad (6)$$

where the coefficient  $g_m$  is given in the weak-coupling limit as

$$g_m^{\text{wc}} = \frac{7\zeta(3)N(0)(\gamma\hbar)^2}{48[(1 + F_0^a)\pi k_B T_c]^2} \quad (7)$$

with the gyromagnetic ratio  $\gamma = -2.04 \times 10^5 / (\text{mT}\cdot\text{sec})$  and the Landau parameter  $F_0^a = -0.695$  at zero pressure. The pressure dependence of  $g_m$  was also reported in Ref.<sup>19</sup>, where  $g_m$  is close to its weak-coupling value  $g_m^{\text{wc}}$  in  $0 \leq p \leq 3.44$  MPa. Thus, we assume  $g_m = g_m^{\text{wc}}$  in the following calculation. The characteristic strength of the magnetic field is  $H_0 = \sqrt{\alpha/g_m^{\text{wc}}} \simeq 0.79\sqrt{t}$  [T]. We ignore the first order contribution of the magnetic field to the GL free energy, since it is sizable at a strong magnetic field  $\sim 1$  T which stabilizes the A<sub>1</sub> phase, while our interest is under a weaker magnetic field on the order of 100 mT. Also, we drop the contribution of the dipole energy which provides negligible contribution to our free energy.

## B. Bulk energy density

To introduce the basic scales in our problem, let us look at the equilibrium property of the bulk <sup>3</sup>He-B phase without a magnetic field. The B-phase order parameter is written as  $A^{(\text{B})} = \Delta_B R(\hat{n}, \phi)$ , where  $\Delta_B$  is the bulk gap amplitude and  $R(\hat{n}, \phi)$  is the rotation matrix with an angle  $\phi$  around the axis  $\hat{n}$ ; the bulk energy is degenerate with respect to  $\hat{n}$  and  $\phi$ . Choosing  $\phi = 0$ , we have  $A^{(\text{B})} = \Delta_B \hat{I}$  with the  $3 \times 3$  unit matrix  $\hat{I}$ . The energy density for the bulk <sup>3</sup>He-B phase is given by

$$f_B^0 = -3\alpha\Delta_B^2 + (9\beta_{12} + 3\beta_{345})\Delta_B^4, \quad (8)$$

where  $\beta_{ij} = \beta_i + \beta_j$  and  $\beta_{ijk} = \beta_i + \beta_j + \beta_k$ . Minimization of this energy density leads to the bulk gap

$$\Delta_B = \sqrt{\frac{\alpha}{\beta'}}, \quad (9)$$

and the corresponding energy density

$$f_B^0 = -\frac{3\alpha^2}{2\beta'} \quad (10)$$

with  $\beta' = 6\beta_{12} + 2\beta_{345}$ .

In this work, a magnetic field  $\mathbf{H} = H\mathbf{e}_i$  is applied along the direction which is parallel ( $i = z$ ) and perpendicular ( $i = x$ ) to the vortex axis. We refer to the former and latter fields as a longitudinal and a transverse magnetic fields, respectively. The magnitude of  $H$  is assumed to be small enough so that the system does not escape from the B-phase. To find the suitable range of  $H$ , we calculate

TABLE II. List of the coefficients for the fitting of the correction of  $\beta_j$  according to the paper by Choi et al.<sup>19</sup> Write “Set II”.

$j$	$B_j^{(0)}$	$B_j^{(1)}$	$B_j^{(2)}$	$B_j^{(3)}$	$B_j^{(4)}$	$B_j^{(5)}$	$B_j^{(6)}$	$B_j^{(7)}$	$B_j^{(8)}$	$B_j^{(9)}$
1	0.030472	0.018587	-0.34839	1.0919	-1.66	1.4058	-0.69863	0.2027	-0.031801	0.0020847
2	-0.11014	0.61315	-1.4457	1.8258	-1.5064	0.84442	-0.31656	0.075439	-0.010271	0.00060559
3	0.10094	-1.7982	4.1219	-6.3112	6.4351	-4.2344	1.7664	-0.45099	0.06427	-0.0039131
4	-0.15024	-1.5428	2.8253	-3.82	3.9311	-2.858	1.3449	-0.3822	0.059274	-0.0038433
5	0.16064	0.25229	-0.79652	1.4591	-1.9474	1.655	-0.84977	0.25472	-0.04103	0.0027444

the bulk free energy in the magnetic field  $\mathbf{H} = H\mathbf{e}_z$ . The order parameter of the B-phase is modified as

$$A^{(B)} = \begin{pmatrix} \Delta_{\perp} & 0 & 0 \\ 0 & \Delta_{\perp} & 0 \\ 0 & 0 & \Delta_{\parallel} \end{pmatrix}, \quad (11)$$

where

$$\Delta_{\perp} = \Delta_B \sqrt{1 + \frac{\beta_{12}g_m}{\alpha\beta_{345}}H^2}$$

$$\Delta_{\parallel} = \Delta_B \sqrt{1 - \frac{(2\beta_{12} + \beta_{345})g_m}{\alpha\beta_{345}}H^2}, \quad (12)$$

and the corresponding energy density is

$$f_B^0 = -\frac{3\alpha^2}{2\beta'} \left[ 1 - \frac{2g_m H^2}{3\alpha} + \frac{(2\beta_{12} + \beta_{345})g_m^2 H^4}{3\alpha^2\beta_{345}} \right]. \quad (13)$$

This energy is compared with that of the bulk A-phase characterized by  $A^{(A)} = \Delta_A \hat{\mathbf{d}}(\hat{\mathbf{m}} + i\hat{\mathbf{n}})$  with arbitrary unit vectors  $\hat{\mathbf{d}}$ ,  $\hat{\mathbf{m}}$ , and  $\hat{\mathbf{n}}$  such that  $\hat{\mathbf{m}} \cdot \hat{\mathbf{n}} = 0$ . By choosing  $\hat{\mathbf{d}} = \hat{\mathbf{e}}_x$ ,  $\hat{\mathbf{m}} = \hat{\mathbf{e}}_x$ , and  $\hat{\mathbf{n}} = \hat{\mathbf{e}}_y$ , the energy does not depend on the magnetic field; the order parameter and energy density are then given by

$$\Delta_A = \sqrt{\frac{\alpha}{4\beta_{245}}}, \quad f_A^0 = -\frac{\alpha^2}{4\beta_{245}}. \quad (14)$$

By comparing the energies  $f_B^0$  and  $f_A^0$ , we obtain the bulk phase diagram in the  $p$ - $H$  plane as shown in Fig. 2. We see qualitatively similar phase diagrams for both data sets of the strong-coupling correction, where the B-phase is stable for a low pressure and a low magnetic field. The area of the stable region of the B-phase for Set II is smaller than that for Set I. Below we confine ourselves within the range  $H \lesssim 0.4H_0$  in which the bulk B-phase is still local energy minimum for high pressure.

### C. Numerics and boundary condition

We compute the order parameters of vortex states by minimizing the total free energy,

$$F = \int d\mathbf{r} (f_B + f_G + f_M) \quad (15)$$

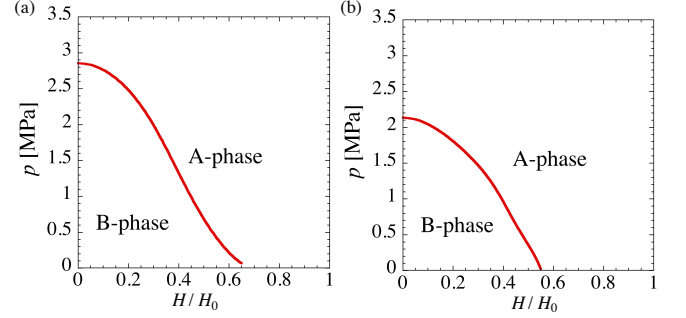


FIG. 2. (Color online) Bulk phase diagram of superfluid  ${}^3\text{He}$  in the  $p$ - $H$  plane, calculated by the GL free energy, with Set I (a) and Set II (b) for strong-coupling corrections.

with the vortex boundary condition. To this end, we evolve the order parameter through the relation

$$\frac{\partial A_{\mu i}}{\partial \tau} = -\frac{\delta F}{\delta A_{\mu i}^*} \quad (16)$$

in two-dimensional Cartesian coordinate, assuming homogeneity along the  $z$ -direction. Equation (16) is known as the time-dependent GL equation; from a suitable initial state, the order parameter converges to the solution of the energy minimum by time-evolving Eq. (16). Here,  $\tau$  is called the imaginary time. Axisymmetry cannot be assumed *a priori* because the  $d$ -vortex breaks it spontaneously.

We use the temperature-dependent coherence length  $\xi(t) = \sqrt{K/\alpha(t)}$ ,  $\Delta_B$  in Eq. (9), and  $|f_B^0|$  in Eq. (10) to scale the length, the order parameter, and the energy density, respectively. Then, the dimensionless order parameter and the free energy is written as  $\tilde{A}_{\mu i} = A_{\mu i}/\sqrt{\alpha(t)}/\beta'$  and

$$\tilde{F} \equiv \frac{F}{|f_B^0|\xi^2(t)} = \int d\tilde{\mathbf{r}} \frac{2}{3} (\tilde{f}_B + \tilde{f}_G + \tilde{f}_M), \quad (17)$$

respectively, where tildes denote the dimensionless variables. Also, by scaling the magnetic field as  $H = H_0\tilde{H}$ , the energy density in the right hand side of Eq. (17) can be written by just replacing the coefficients in Eqs. (2),

(4), and (6) as

$$\alpha \rightarrow 1, \quad \beta_j \rightarrow \frac{\beta_j}{\beta'} = \frac{\beta_j^{\text{wc}} + \Delta\beta_j}{\beta'},$$

$$K \rightarrow 1, \quad g_m \rightarrow \frac{g_m(p)}{g_m(0)} \approx 1. \quad (18)$$

Then, all physical quantities become dimensionless.

We take a system size for numerical simulations as  $\tilde{x}, \tilde{y} \in [-50, 50]$  with a  $500 \times 500$  numerical grid. Although we solve Eq. (16) in the  $xy$ -coordinate, we impose the Dirichlet boundary condition for the vortex structure on the cylinder with the radius  $\tilde{R} = 50$ . The boundary condition is taken as  $\lim_{\tilde{r} \rightarrow \tilde{R}} \tilde{A}_{\mu i}(\tilde{r}, \theta) = \hat{I} e^{i\theta}$ , where  $(\tilde{r}, \theta)$  is the dimensionless polar coordinate. This means that far from the vortex core at the center, the order parameter approaches to the bulk value with unit phase winding. However, as shown by Hasegawa,<sup>21</sup> the asymptotic form of the off-diagonal components of  $\tilde{A}_{\mu i}$ , some of which occupy the vortex core, decays slowly as  $\sim r^{-1}$ , and we have to take large system size to ensure the validity of this boundary condition. We confirm that  $\tilde{R} = 50$  is large enough to ignore the finite size effect on the vortex energy. Furthermore we avoid the unfavorable boundary contribution to the vortex energy by integrating Eq. (17) within the region  $\tilde{R} \leq 40$  when calculating the total energy.

#### D. Vortex state without a magnetic field

Here, we briefly review the vortex state without a magnetic field. Typically, there are three types of solutions, known as the  $o$ -vortex, the  $v$ -vortex, and the  $d$ -vortex. Thuneberg analyzed these vortex states and calculated their energies within the GL theory with  $\beta$ -values obtained from Set I.<sup>10,11</sup> Here, we calculate them not only with Set I but also with Set II, obtaining qualitatively similar results for both data sets; the typical spatial profiles of the order parameters for Set II are shown in Fig. 3 and the vortex energy as a function of  $p$  is shown in Fig. 4. The  $o$ -vortex has an axisymmetric structure and the core is not filled with any superfluid components. The  $v$ -vortex is also axisymmetric but has a core filled mainly with the A-phase components  $\text{Re}(\tilde{A}_{zx})$  and  $\text{Im}(\tilde{A}_{zy})$ , whose amplitudes take the same value at the origin. There are also minor components  $\text{Re}(\tilde{A}_{xz})$  and  $\text{Im}(\tilde{A}_{yz})$  filling the vortex core, which are known as the  $\beta$ -phase. The fraction of the A-phase component increases as the pressure increases. The  $d$ -vortex is a non-axisymmetric vortex as seen in Figs. 3(c-x) and (c-y), where the profiles are different along the  $\tilde{x}$ -direction and  $\tilde{y}$ -direction. The core components are  $\text{Re}(\tilde{A}_{zx})$  and  $\text{Re}(\tilde{A}_{xz})$ , corresponding to the planar phase characterized by  $\tilde{A} = \tilde{\Delta}_p R(\hat{n}, \phi)(I - \hat{w}\hat{w})$  with  $\hat{n} = \hat{w} = \mathbf{e}_y$  and  $\phi = \pi/2$ .<sup>11</sup> In this case, there appear double vortex cores along the  $y$ -direction. The vortex energy is calculated by

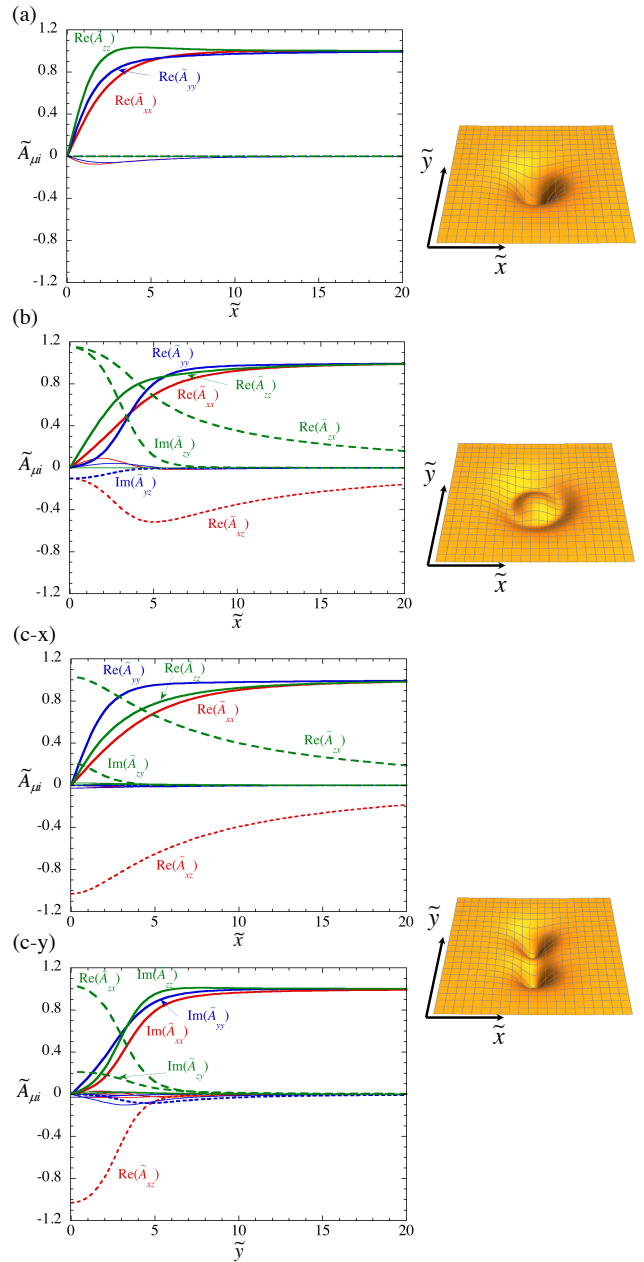


FIG. 3. (Color online) Left: Typical radial profiles of the order parameters for (a) the  $o$ -vortex, (b) the  $v$ -vortex, and (c) the  $d$ -vortex. Here the strong-coupling correction Set II is employed and the pressure is set to 3.0 MPa. Because the  $d$ -vortex is not axisymmetric, we show the profiles along the  $x$ - and  $y$ -axis as (c-x) and (c-y), respectively. Diagonal components of  $(\tilde{A}_{\mu i})$  are shown in solid curves, while off-diagonal ones in dashed curves. Right: Corresponding 2D profiles of the pair density  $\sum_{\mu,i} |\tilde{A}_{\mu i}|^2$ .

subtracting  $\tilde{F}_{\text{bulk}}$  and  $\tilde{F}_{\text{hyd}}$  from the total free energy  $\tilde{F}$  in Eq. (17) as

$$\tilde{F}_{\text{vortex}} = \tilde{F} - \tilde{F}_{\text{bulk}} - \tilde{F}_{\text{hyd}}. \quad (19)$$

Here,  $\tilde{F}_{\text{bulk}} = 1 \times S$  is the bulk free energy with the system area  $S$  and  $F_{\text{hyd}} = \int d\mathbf{r} \sum_k \rho_k v_k^2 / 2$  is a hydrodynamic kinetic energy caused by vortex flow. The energy  $F_{\text{hyd}}$  can be calculated by combining the relation  $j_k = \rho_k v_{sk}$  ( $k = x, y, z$ ) for the superfluid density  $\rho_k$  and the current density

$$j_k = \frac{4m_3 K}{\hbar} \text{Im} [A_{\mu k}^* \partial_j A_{\mu j} + A_{\mu j}^* \partial_k A_{\mu j} + A_{\mu j}^* \partial_j A_{\mu k}]. \quad (20)$$

The dimensionless form of  $F_{\text{hyd}}$  is  $\tilde{F}_{\text{hyd}} = (20\pi/3) \ln(R/\xi(t))$  with the radius  $R$  of the cylinder, where the lower bound of the integral has been taken as  $\xi(t)$ .

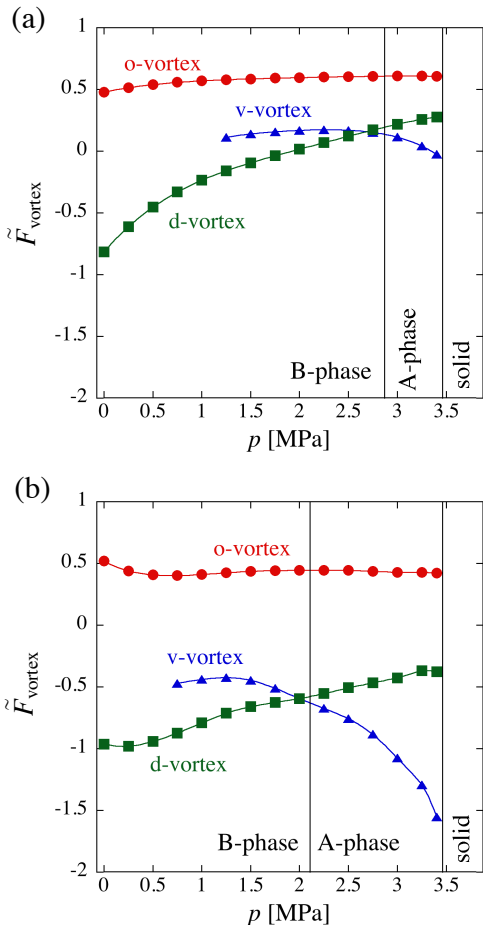


FIG. 4. (Color online) Free energies of the three vortex states without a magnetic field as functions of the pressure  $p$  for Set I (a) and Set II (b). The energies of the  $o$ -,  $v$ -, and  $d$ -vortices are shown by curves with red circles, blue triangles, and green squares, respectively. The bulk A-B phase boundary is taken from Fig. 2.

For Set I, we reproduce the results of Thuneberg<sup>10,11</sup> as seen in Fig. 4(a) and confirm the validity of our calculation. The  $o$ -vortex is always the highest energy configuration. For low pressures, the  $d$ -vortex is the most stable vortex state, while the  $v$ -vortex is most stable above

$p \simeq 2.7$  MPa. In our two-dimensional calculation without axisymmetry, the  $v$ -vortex is energetically unstable for low pressures below 1.25 MPa and it decays to the  $d$ -vortex. The similar behavior has also been mentioned by Thuneberg.<sup>11</sup>

Figure 4(b) shows the energy of the vortex states for Set II. Although the result qualitatively agrees with that in Fig. 4(a), we confirm quantitative differences. Especially, the critical pressure for the transition between the  $v$ -vortex and the  $d$ -vortex is remarkably reduced to  $\approx 2.0$  MPa, compared to that of  $\approx 2.7$  MPa seen in Fig. 4(a). Thus, the results for Set II explains the experimental observation of the vortex-core transition<sup>3,10</sup> for  $T \simeq T_c$  more accurately than those for Set I. Note that the transition pressure of the  $v$ - and the  $d$ -vortices is close to the boundary of the bulk AB transition for both Set I and Set II.

### III. VORTEX STATE UNDER A MAGNETIC FIELD

In this section, we consider the effect of a magnetic field  $\mathbf{H}$  on the vortex states. We address two situations: one with the longitudinal magnetic field  $\mathbf{H} = H\mathbf{e}_z$ , and the other with the transverse magnetic field  $\mathbf{H} = H\mathbf{e}_x$ .

#### A. Longitudinal magnetic field

Here we consider the vortices under a magnetic field along the  $z$ -axis. The effect of the axial magnetic field can be understood by examining the free energy functional. The quadratic magnetic-field term Eq. (6) for  $\mathbf{H} = H\mathbf{e}_z$  is written as  $\tilde{f}_M = \tilde{H}^2 \sum_i |\tilde{A}_{zi}|^2$ . Thus, the population of the core components whose spin is along the  $z$ -direction in the  $v$ - and  $d$ -vortices should be suppressed to reduce the energy cost. Then, it is not trivial to tell which vortex state has the lowest energy.

To obtain the vortex solution under the magnetic field, we should fix the boundary condition, i.e., the proper choice of  $R(\hat{\mathbf{n}}, \phi)$  at the boundary. In the bulk region, by taking account of the quadratic magnetic energy and the dipole-dipole energy, the  $\hat{\mathbf{n}}$  should be parallel to  $\mathbf{H}$ , since the combination of these energies gives an energy contribution  $\propto -(\hat{\mathbf{n}} \cdot \mathbf{H})^2$ .<sup>11</sup> Also, the dipole-dipole energy fixes  $\phi = \arccos(-1/4)$ . Since the vortices are along the  $z$ -axis in our problem, the vortex structures including the core components as well as the vortex energies are not affected by the rotation  $R(\hat{\mathbf{z}}, \phi)$  of the order parameter at the boundary. Thus, we set the bulk amplitude with  $\phi = 0$  as the Dirichlet boundary condition at  $r = R$ , and write the order parameter at the boundary as

$$\tilde{A}^{(B)} = \begin{pmatrix} \tilde{\Delta}_\perp & 0 & 0 \\ 0 & \tilde{\Delta}_\perp & 0 \\ 0 & 0 & \tilde{\Delta}_\parallel \end{pmatrix} e^{i\theta}, \quad (21)$$

where  $\tilde{\Delta}_\perp$  and  $\tilde{\Delta}_\parallel$  are given by Eqs. (12). The vortex energy  $\tilde{F} - \tilde{F}_{\text{bulk}} - \tilde{F}_{\text{hyd}}$  is calculated in a similar way as that described in Sec. IID. Here,  $\tilde{F}_{\text{bulk}}$  is evaluated by the spatial integral of Eq. (13) and  $\tilde{F}_{\text{hyd}} = (4\pi/3)(4\tilde{\Delta}_\perp^2 + \tilde{\Delta}_\parallel^2) \ln(R/\xi(t))$ .

Figure 5 shows the vortex free energy  $\tilde{F}_{\text{vortex}}$  of the three vortex states as a function of the pressure for several  $\tilde{H}$ . The main feature of Fig. 5 for both sets of the strong-coupling correction is that the  $d$ -vortex is the most preferable structure under the magnetic field. The  $v$ -vortex has a local minimum only in a high-pressure region, which shrinks and eventually disappears as the magnetic field strength increases; the initial  $v$ -vortex relaxes to the  $d$ -vortex through the evolution of Eq. (16) when  $v$ -vortex is unstable. The  $o$ -vortex is always the highest energy state, being metastable in all situations. Although we solved Eq. (16) with other initial configurations, the final states of the imaginary time evolution are always one of the three vortices.

Let us see the details of the magnetic field dependence of the  $v$ - and the  $d$ -vortices in high pressure region. The free energy of the  $v$ -vortex increases with  $H$ , while that of the  $d$ -vortex decreases, as shown in Fig. 5(d). This inverts the energetic stability of the two vortex states at a critical magnetic field. Figure 6 shows the phase diagram of the stability of the  $v$ - and the  $d$ -vortices. In addition to the above critical magnetic field, there is another one which gives metastability of the  $v$ -vortex. These critical magnetic fields monotonically increase with the pressure.

The  $p$ -dependence of the critical magnetic field can be qualitatively understood by comparing the free energy of the bulk A phase and that of the planar phase. The vortex core is filled with these phases. For the A phase in the core of the  $v$ -vortex, described by  $\text{Re}(\tilde{A}_{zx}) = \text{Im}(\tilde{A}_{zy}) \equiv \tilde{\Delta}_{A1}$ , the bulk amplitude and the minimized energy are given by

$$\begin{aligned}\tilde{\Delta}_{A1}^2 &= \frac{\beta'(1 - \tilde{H}^2)}{4\beta_{245}}, \\ \tilde{f}_A^H &= -\frac{\beta'(1 - \tilde{H}^2)^2}{6\beta_{245}}.\end{aligned}\quad (22)$$

Here, we ignore the minor  $\beta$ -phase components for simplicity. For the planar phase in the  $d$ -vortex, we take the components  $\text{Re}(\tilde{A}_{zx}) \equiv \tilde{\Delta}_{p1}$  and  $\text{Re}(\tilde{A}_{xz}) \equiv -\tilde{\Delta}_{p2}$ , and the bulk amplitude and the minimized energy are

$$\begin{aligned}\tilde{\Delta}_{p1}^2 &= \frac{\beta'[\beta_{345} - \tilde{H}^2(\beta_{12} + \beta_{345})]}{2\beta_{345}(2\beta_{12} + \beta_{345})}, \\ \tilde{\Delta}_{p2}^2 &= \frac{\beta'(\beta_{12}\tilde{H}^2 + \beta_{345})}{2\beta_{345}(2\beta_{12} + \beta_{345})}, \\ \tilde{f}_p^H &= -\frac{\beta'[\beta_{345}(2 - 2\tilde{H}^2 + \tilde{H}^4) + \beta_{12}\tilde{H}^4]}{6\beta_{345}(2\beta_{12} + \beta_{345})}.\end{aligned}\quad (23)$$

For a given pressure,  $\tilde{f}_p^H$  becomes lower than  $\tilde{f}_A^H$  at a certain magnetic field, which is shown by a thin dashed

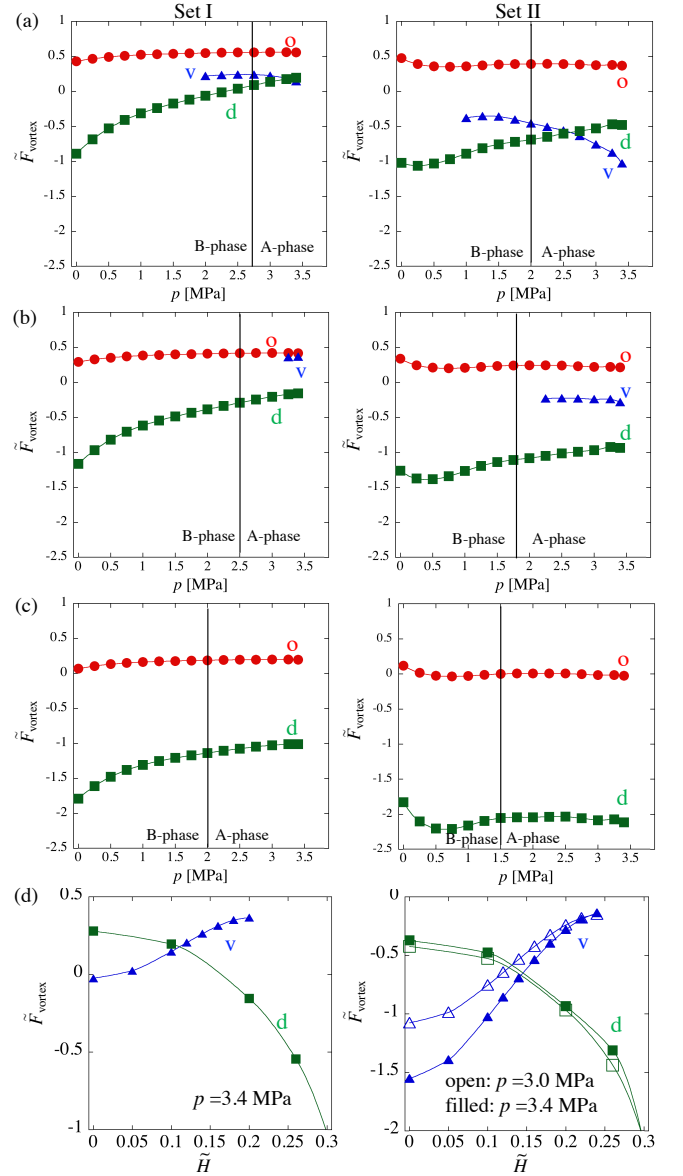


FIG. 5. (Color online) Free energies of the three vortex states as functions of pressure  $p$  for Set I (left panels) and Set II (right panels). The magnitude of the magnetic field is (a)  $\tilde{H} = 0.1$ , (b)  $\tilde{H} = 0.2$ , (c)  $\tilde{H} = 0.3$ . The energies of the  $o$ -,  $v$ -, and  $d$ -vortices are shown by curves with red circles, blue triangles, and green squares, respectively. The bulk A-B phase boundary is taken from Fig. 2. The figures (d) show the free energies of  $v$ - and  $d$ -vortices as functions of  $\tilde{H}$  at high pressure region; we show the plots with  $p = 3.0$  MPa for Set I, and with  $p = 3.0$  and  $3.4$  MPa for Set II.

curve in the phase diagram of Fig. 6. The dashed curve has a similar pressure dependence as the critical magnetic fields described above. Thus, we expect that the occupation of the planar-phase component is energetically favorable than the A-phase component in the vortex core in the presence of a longitudinal magnetic field.

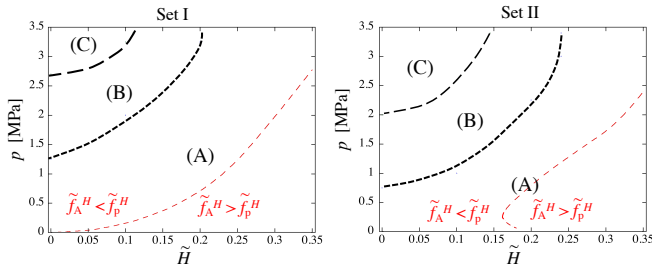


FIG. 6. (Color online)  $p$ - $H$  phase diagram of the stable  $v$ - and  $d$ -vortex states for (a) Set I and (b) Set II of the strong-coupling corrections. The regions of the phase diagram are separated into (A):  $v$ -vortex is unstable and  $d$ -vortex is stable, (B):  $v$ -vortex is metastable and  $d$ -vortex is stable, (C):  $v$ -vortex is stable and  $d$ -vortex is metastable. The (red) thin-dashed curve represents the phase boundary of the bulk A-phase and bulk planar-phase, which is obtained by comparing the free energies Eqs. (22) and (23).

### B. Transverse magnetic field

We turn to the analysis on the vortices in the transverse magnetic field. Let us consider  $\tilde{\mathbf{H}} = H\mathbf{e}_x$ . Then, the magnetic free energy written as  $\tilde{f}_M = \tilde{H}^2 \sum |\tilde{A}_{xi}|^2$  leads to suppression of the components  $|\tilde{A}_{xi}|$ . Here, we should take the boundary condition

$$R(\hat{\mathbf{x}}, \phi)\tilde{A}^{(B)}e^{i\theta} = \begin{pmatrix} \tilde{\Delta}_{\parallel} & 0 & 0 \\ 0 & \tilde{\Delta}_{\perp} \cos \phi & -\tilde{\Delta}_{\perp} \sin \phi \\ 0 & \tilde{\Delta}_{\perp} \sin \phi & \tilde{\Delta}_{\perp} \cos \phi \end{pmatrix} e^{i\theta} \quad (24)$$

at the boundary  $r = R$ , where  $\tilde{A}^{(B)} = \text{diag}(\tilde{\Delta}_{\parallel}, \tilde{\Delta}_{\perp}, \tilde{\Delta}_{\perp})$  with Eq. (12). Then, it is not trivial how the rotation angle  $\phi$  at the boundary affects the vortex structures, because the components  $\tilde{A}_{yz}$  and  $\tilde{A}_{zy}$  appearing in the vortex cores are influenced by the choice of the angle  $\phi$ . More precisely, when  $\phi \neq 0$ , not only the components  $\tilde{A}_{yy}$  and  $\tilde{A}_{zz}$  but also  $\tilde{A}_{yz}$  and  $\tilde{A}_{zy}$  should have zeros around the origin for the nonzero winding number. We confirm that the character of all vortices are independent of  $\phi$  as shown later; the internal structure of the vortex core adjusts to the given boundary condition without changing the free energy.

Here, we analyze the vortex structure by employing the boundary condition Eq. (24) with  $\phi = 0$ . There are two main effects of  $\tilde{\mathbf{H}} = H\mathbf{e}_x$  on the core structures. One is the stabilization of the  $v$ -vortex. The other is to lock the orientation of the double cores of the  $d$ -vortex along the  $x$ - or  $y$ -direction; we refer to the former and the latter as  $d_x$ -vortex and  $d_y$ -vortex, respectively. Figure 7 shows the vortex energy  $\tilde{F}_{\text{vortex}}$  as a function of the pressure, while Fig. 8 depicts a magnified view of Fig. 7 in the vicinity of the transition point by taking only the energies of the  $v$ -,  $d_x$ -, and  $d_y$ -vortices. For  $\tilde{H} = 0.1$ , the qualitative stability properties of the vortex states are not changed

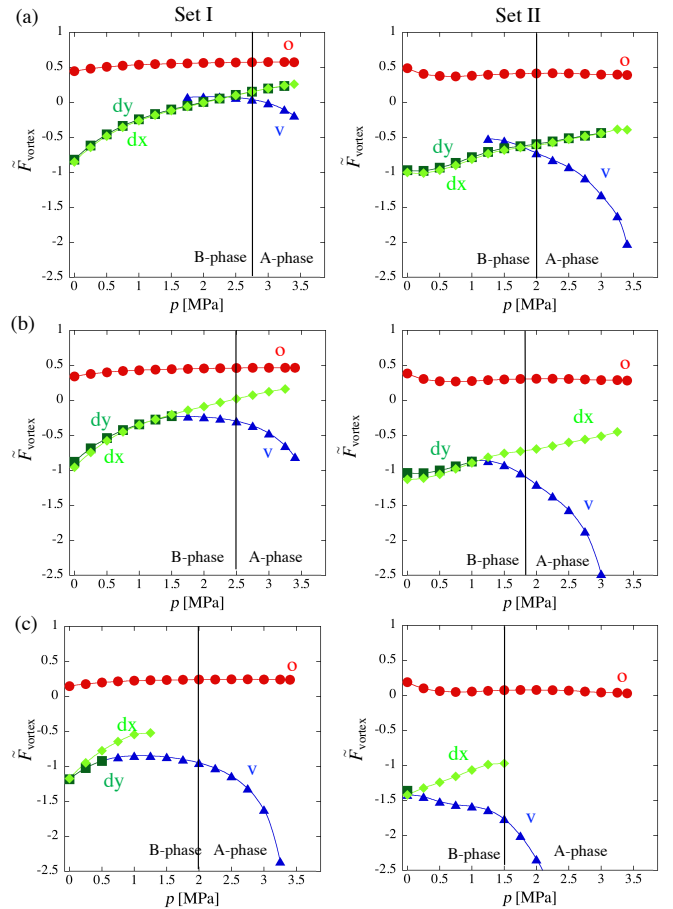


FIG. 7. (Color online) Free energies of the vortex states in the presence of a transverse magnetic field as a function of the pressure  $p$  for Set I (left panels) and Set II (right panels). The magnitude of the magnetic field is (a)  $\tilde{H} = 0.1$ , (b)  $\tilde{H} = 0.2$ , (c)  $\tilde{H} = 0.3$ . The energies of the  $o$ -,  $v$ -,  $d_y$ - and  $d_x$ - vortices are shown by curves with red circles, blue triangles, green squares, and yellow green diamonds, respectively. The bulk A-B phase boundary is taken from Fig. 2.

from those for  $\tilde{H} = 0$ . However, the energy of the  $d_x$ -vortex is slightly lower than that of the  $d_y$ -vortex. With increasing the magnetic field to  $\tilde{H} = 0.2$ , the stability region of the  $v$ -vortex extends to the lower pressure region. Also, the  $d_y$ -vortex becomes unstable in the high pressure region, decaying into the symmetric  $v$ -vortex. Above  $\tilde{H} = 0.2$ , the  $d_y$ -vortex continuously transforms to the  $v$ -vortex as  $p$  increases. No hysteresis is observed in this transition. The  $d_x$ -vortex is stable in the low-pressure region and survives as a metastable state for higher pressures. With increasing to  $\tilde{H} = 0.3$ , although the  $d_x$ -vortex exists as a metastable state in the low pressure region, the  $v$ -vortex becomes the most stable state. For higher pressures (above 3.25 MPa for Set I and 2.25 MPa for Set II), the vortex state is unstable to become the bulk A-phase without vorticity. Similarly to the results in Sec. III A, the  $o$ -vortex is always metastable.

In order to understand the above properties, it is useful



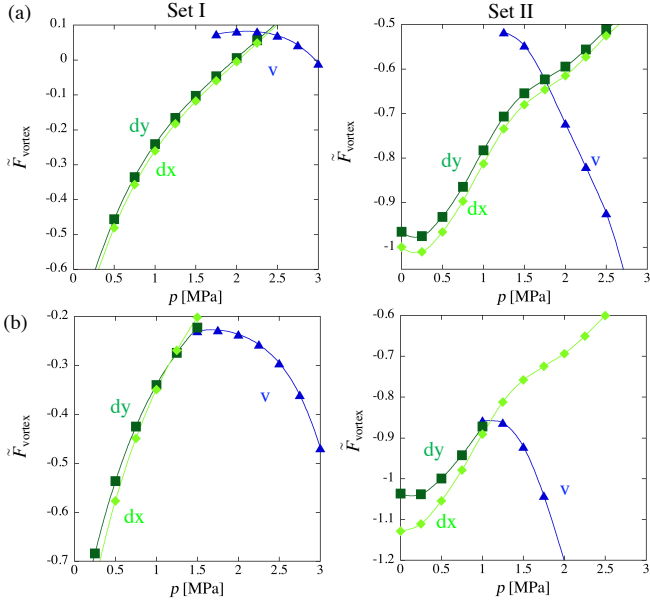


FIG. 8. (Color online) Free energies of the  $v$ -,  $d_y$ -, and  $d_x$ -vortex states in the presence of a transverse magnetic field as a function of the pressure  $p$  for Set I (left panels) and Set II (right panels) for (a)  $\tilde{H} = 0.1$  and (b)  $\tilde{H} = 0.2$ . The figures are the enlarged view of Fig. 7 (a) and (b) in the vicinity of the transition pressure.

to consider the bulk free energy of the core components. The order parameter of the planar phase in the  $d$ -vortex and the rotation angle  $\varphi$  of the orientation of the splitting double-core are related with

$$\tilde{A}^{\text{pl}} = \begin{pmatrix} 0 & 0 & -\tilde{\Delta}_{p2}a(\varphi) \\ 0 & 0 & -\tilde{\Delta}_{p2}b(\varphi) \\ \tilde{\Delta}_{p1}a(\varphi) & \tilde{\Delta}_{p1}b(\varphi) & 0 \end{pmatrix} \quad (25)$$

with  $a(\varphi) = \cos^2 \varphi - i \sin \varphi \cos \varphi$  and  $b(\varphi) = -\sin \varphi \cos \varphi + i \sin^2 \varphi$ . Here,  $\varphi = 0$  and  $\pi/2$  correspond to the  $d_y$ - and  $d_x$ -vortices, respectively, where the profiles of the order parameters are shown in Fig. 3(c) for the  $d_y$ -vortex and Fig. 9 for the  $d_x$ -vortex. Then, the bulk free energy  $f_B$  is independent of  $\varphi$  but the quadratic magnetic free energy for  $\mathbf{H} = H\mathbf{e}_x$  is written as  $\tilde{f}_M = \alpha \tilde{\Delta}_{p2}^2 \tilde{H}^2 \cos^2 \varphi$ . In the bulk, the magnetic free energy is minimized for  $\varphi = \pi/2$ . This feature is consistent with our observation in Fig. 8. We confirm that, through the imaginary time evolution from the initial states with  $0 < \varphi < \pi/2$ , the solutions always converge to those with  $\varphi = 0$  or  $\varphi = \pi/2$ . This implies that there is an energy barrier between  $d_x$ - and  $d_y$ -vortices and the barrier originates from  $\tilde{f}_G$ .

The continuous structural change between the  $d_y$ -vortex and the  $v$ -vortex can be analyzed by carefully examining the core components. For the boundary condition Eq. (24) with  $\phi = 0$ , the distribution of  $\text{Re}(\tilde{A}_{xz})$  and  $\text{Re}(\tilde{A}_{zx})$  in the  $v$ - and  $d_y$ -vortices are similar to each other, which allows the continuous transformation be-

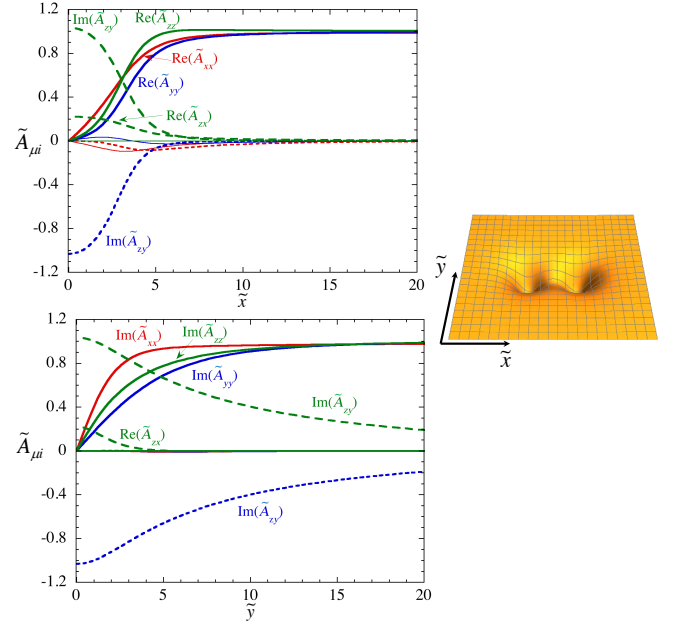


FIG. 9. (Color online) Typical radial profiles of the order parameter (left) and the 2D profile of the pair density  $\sum_{\mu,i} |\tilde{A}_{\mu i}|^2$  (right) of the  $d_x$ -vortex for  $p = 3.0$  MPa and  $\tilde{H} = 0.2$ .

tween the two structures. The angle  $\varphi$  of the double-core has to be rotated by  $\pi/2$  for the  $d_x$ -vortex to have similar distributions of  $\text{Re}(\tilde{A}_{xz})$  and  $\text{Re}(\tilde{A}_{zx})$  with those in the  $v$ -vortex. This is prohibited by the energy barrier stated above and ensures the presence of the metastable  $d_x$ -vortex in the high pressure region as seen in Figs. 7 and 8. The change from the  $d_y$ -vortex to the  $v$ -vortex can be understood by examining the core components at the origin. Figure 10(a) shows the difference  $\text{Re}(\tilde{A}_{zx}) - \text{Im}(\tilde{A}_{zy})$  at the origin as a function of the pressure; the finite difference implies the  $d_y$ -vortex with the planar phase core, while the zero difference signifies the  $v$ -vortex with the A-phase core. For  $\tilde{H} = 0.1$ , there is a hysteresis of the transition between the two vortex states. As  $\tilde{H}$  is increased to 0.2, there appears a jump of the difference without hysteresis. For  $\tilde{H} = 0.3$ , the difference monotonically decreases as  $p$  increases, where the continuous change from the  $d_y$ -vortex to the  $v$ -vortex takes place as  $p$  increases, as shown in Fig. 10(b). We should note that for  $H \neq 0$  the  $v$ -vortex has the finite difference  $\text{Re}(\tilde{A}_{zx}) - \text{Im}(\tilde{A}_{zy})$  in the core components, which should be referred to as the *non-axisymmetric v-vortex*

We checked that the vortex energies are independent of the change of the boundary condition associated with the angle  $\phi$  of Eq. (24). In Fig. 11, we show the profile of the order parameters of  $v$ -,  $d_y$ -, and  $d_x$ -vortices for  $\phi = \pi/4$ . Then, the components  $\tilde{A}_{yy}$ ,  $\tilde{A}_{yz}$ ,  $\tilde{A}_{zy}$ ,  $\tilde{A}_{zz}$  should have zeros around the origin because of the boundary condition with a phase winding, despite the fact that  $\tilde{A}_{yz}$  and  $\tilde{A}_{zy}$  should occupy the vortex core in each vortex

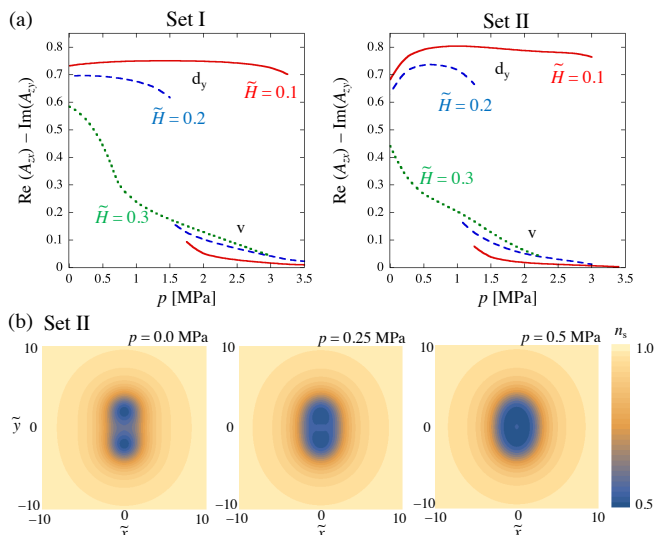


FIG. 10. (Color online) Transition from the  $d_y$ -vortex to the  $v$ -vortex as  $p$  is varied. In (a), the difference  $\text{Re}(\tilde{A}_{zx}) - \text{Im}(\tilde{A}_{zy})$  at the origin  $x = y = 0$  is shown as a function of  $p$  for  $\tilde{H} = 0.1, 0.2, 0.3$ . The left and the right panels correspond to Set I and Set II, respectively. The panels in (b) show the contour plots of the pair density  $\sum_{\mu,i} |\tilde{A}_{\mu,i}|^2$  for  $\tilde{H} = 0.3$  and  $p = 0, 0.25$  and  $0.5$  MPa from left to right with Set II.

state. Figure 11 shows that zeros of the order parameter appear at the positions displaced from the origin along the  $y$ -direction. We find numerically that the total energy as well as the total pair density  $\sum_{\mu,i} |\tilde{A}_{\mu,i}|^2$  are invariant with respect to  $\phi$ .

Finally, our results are summarized in the  $p$ - $H$  phase diagram of Fig. 12. As an overall feature, with increasing the transverse magnetic field  $\tilde{H}$ , the stable region of the  $d$ -vortex gradually shrinks, while that of the  $v$ -vortex gradually expands.

#### IV. CONCLUSION

In this paper, we study the vortex states in superfluid  $^3\text{He}$ -B phase under a longitudinal and a transverse magnetic fields within the GL theory. We calculate the free energy of the  $\sigma$ -, the  $v$ - and the  $d$ -vortices with two different sets of the strong-coupling corrections, Set I and Set II, finding that the results for Set II reproduce quantitatively the experimental data at zero magnetic fields. Under a magnetic field along the  $z$ -axis (the axis of the

vortex), the  $v$ -vortex, which is stable at high pressure and zero magnetic field, becomes unstable and decays to the  $d$ -vortex. On the other hand, if the magnetic field is applied along the  $x$ -axis, perpendicular to the axis of the vortex, the  $v$ -vortex is the most stable state at high magnetic field. In the latter case, anisotropic feature of the vortex structure is more remarkable, where the  $d_x$ - and the  $d_y$ -vortices exist as distinct energy minima. We estimate that these transitions take place at  $H \sim 0.2H_0 \sim 50$  mT, when  $T = 0.9T_c$ , which is observable under suitable experimental setup.<sup>3,9,13</sup>

The dependence of the vortex structure on the magnetic field can be understood qualitatively by the energetic argument of the core-occupying components of the order parameter. A magnetic field applied to a bulk superfluid  $^3\text{He}$  stabilizes the A-phase more than the B-phase in general. The  $d$ -vortex tends to be stabilized in the presence of a magnetic field along the  $z$ -axis. Recall that the core of the  $v$ -vortex is filled with the A-phase with non-vanishing order parameter components  $A_{zi}$  ( $i = x, y$ ), which are suppressed by the magnetic field along the  $z$ -axis. This makes the  $v$ -vortex energetically unfavorable compared to the  $d$ -vortex. This is rather counterintuitive since a magnetic field stabilizes the bulk A-phase. A magnetic field along the  $x$ -axis suppresses the order parameter components  $A_{xi}$  ( $i = x, y, z$ ). The core of the  $v$ -vortex is filled with the components  $A_{zx}$  and  $A_{zy}$  while that of the  $d_x$ -vortex, the stable  $d$ -vortex in this case, is filled with the planar phase with dominant components  $\text{Im}A_{yz}$  and  $\text{Im}A_{zy}$ . These core components are not suppressed by the transverse magnetic field. However, the  $v$ -vortex is more stable than the  $d_x$ -vortex when the transverse magnetic field is strong enough since a magnetic field energetically favors the A-phase compared to the planar phase for a bulk superfluid  $^3\text{He}$ . As a further study, it is interesting to see the effect of a magnetic field applied obliquely to the vortex axis.

#### ACKNOWLEDGMENTS

We would like to thank Erkki Thuneberg and Matti Krusius for their interest in this work. The work of K.K. is partly supported by KAKENHI from the Japan Society for the Promotion of Science (JSPS) Grant-in-Aid for Scientific Research (KAKENHI Grant No. 18K03472). The work of M.N. is partly supported by KAKENHI from the JSPS Grant-in-Aid for Scientific Research (KAKENHI Grant No. 17K05554).

<sup>1</sup> D. Vollhardt and P. Wölfle, *The Superfluid phase of Helium 3* (Taylor and Francis, London, 1990).

<sup>2</sup> M. M. Salomaa and G. E. Volovik, Quantized vortices in superfluid  $^3\text{He}$ , *Rev. Mod. Phys.* **59** 533 (1987).

<sup>3</sup> M. Krusius, The Vortices of Superfluid  $^3\text{He}$ , *J. Low Temp. Phys.* **91** 233 (1993).

<sup>4</sup> M. M. Salomaa and G. E. Volovik, Vortices with Ferro-magnetic Superfluid Core in  $^3\text{He}$ -B, *Phys. Rev. Lett.* **51**,

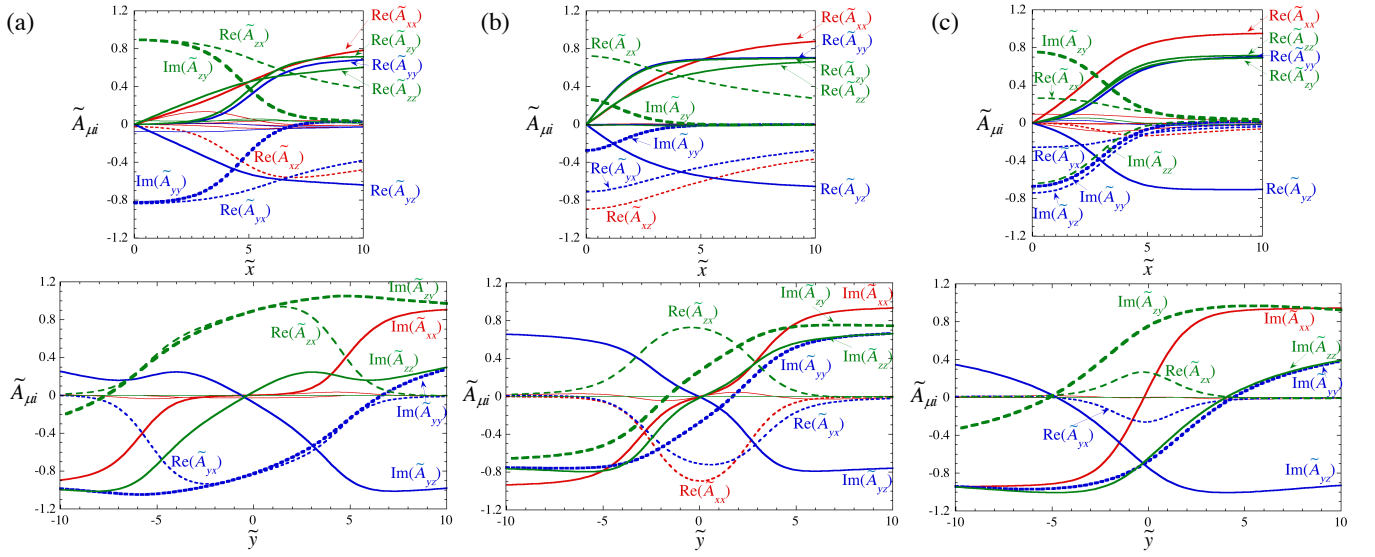


FIG. 11. (Color online) The cross section of the order parameter  $A$  along the  $x$ - (top) and the  $y$ - (bottom) axes for (a) the  $v$ -vortex ( $p = 3.0$  MPa), (b) the  $d_y$ -vortex ( $p = 0.0$  MPa), and (c) the  $d_x$ -vortex ( $p = 0.0$  MPa) for  $\tilde{H} = 0.2$ , obtained with the boundary condition Eq. (24) with  $\phi = \pi/4$ . In all cases, the distributions of the core components along the  $x$ -axis have inversion symmetry at the origin, but those along the  $y$ -direction do not.

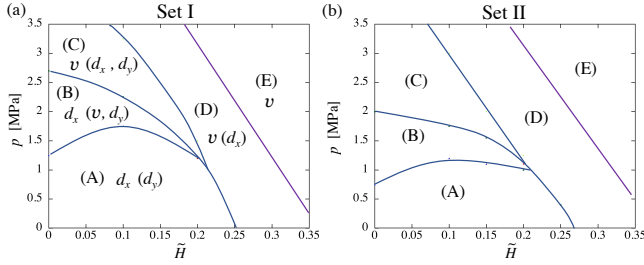


FIG. 12. (Color online)  $p$ - $H$  phase diagram of the stable  $v$ - and  $d$ -vortex states for (a) Set I and (b) Set II of the strong-coupling corrections. The  $p$ - $H$  plane is divided into (A): the  $d_x$ -vortex is stable and the  $d_y$ -vortex is metastable, (B): the  $v$ -vortex is metastable, the  $d_x$ -vortex is stable, and the  $d_y$ -vortex is metastable, (C): the  $v$ -vortex is stable and the  $d_x$ - and  $d_y$ -vortices are metastable, (D): the  $v$ -vortex is stable and the  $d_x$ -vortex is metastable, and (E): the  $v$ -vortex is stable.

2040 (1983).

- <sup>5</sup> M. M. Salomaa and G. E. Volovik, Symmetry and structure of quantized vortices in superfluid  $^3\text{He-B}$ , Phys. Rev. B **31** 203 (1985).
- <sup>6</sup> T. Ohmi, T. Tsuneto, and T. Fujita, Core structure of Vortex Line in  $^3\text{He-B}$ , Prog. Theor. Phys. **70**, 647 (1983).
- <sup>7</sup> S. Theodorakis and A. Fetter, Vortices and NMR in Rotating  $^3\text{He-B}$ , J. Low Temp. Phys. **52**, 559 (1983).
- <sup>8</sup> T. Passvogel, L. Tewordt, and N. Schopohl, Stability, Orientation Effects, and Temperature Dependence of Nonunitary Vortex Structures in Superfluid  $^3\text{He}$ , J. Low Temp. Phys. **56**, 383 (1984).
- <sup>9</sup> P. J. Hakonen, M. Krusius, M. M. Salomaa, J. T. Simola, Y. M. Bunkov, V. P. Mineev, and G. E. Volovik, Magnetic Vortices in Rotating Superfluid  $^3\text{He-B}$ , Phys. Rev. Lett. **51**, 1362 (1983).

- <sup>10</sup> E. V. Thuneberg, Identification of Vortices in Superfluid  $^3\text{He-B}$ , Phys. Rev. Lett. **56**, 359 (1986).
- <sup>11</sup> E. V. Thuneberg, Ginzburg-Landau theory of vortices in superfluid  $^3\text{He-B}$ , Phys. Rev. B **36** 3583 (1987).
- <sup>12</sup> M. M. Salomaa and G. E. Volovik, Vortices with Spontaneously Broken Axisymmetry in  $^3\text{He-B}$ , Phys. Rev. Lett. **56** 363 (1986).
- <sup>13</sup> Y. Kondo, J. S. Korhonen, M. Krusius, V. V. Dmitriev, Y. M. Mukharsky, E. B. Sonin, and G. E. Volovik, Direct Observation of the Nonaxisymmetric Vortex in Superfluid  $^3\text{He-B}$ , Phys. Rev. Lett. **67**, 81 (1991).
- <sup>14</sup> M. Fogelström and J. Kurkijärvi, Quasiclassical Theory of Vortices in  $^3\text{He-B}$ , J. Low Temp. Phys. **98**, 195 (1995); **116**, 1 (1999).
- <sup>15</sup> Y. Tsutsumi, T. Kawakami, K. Shiozaki, M. Sato, K. Machida, Symmetry-protected vortex bound state in superfluid  $^3\text{He-B}$  phase, Phys. Rev. B **91**, 144504 (2015).
- <sup>16</sup> M. A. Silaev, E. V. Thuneberg, and M. Fogelström, Lifshitz Transition in the Double-Core Vortex in  $^3\text{He-B}$ , Phys. Rev. Lett. **115**, 235301 (2015).
- <sup>17</sup> J. A. Sauls and J. W. Serene, Comment on “Symmetry and structure of quantized vortices in superfluid  $^3\text{He-B}$ ”, Phys. Rev. B **32**, 4782 (1985).
- <sup>18</sup> J. A. Sauls and J. W. Serene, Potential-scattering models for the quasiparticle interactions in liquid  $^3\text{He}$ , Phys. Rev. B **24** 183 (1981).
- <sup>19</sup> H. Choi, J. P. Davis, J. Pollanen, T. M. Haard, and W. P. Halperin, Strong coupling corrections to the Ginzburg-Landau theory of superfluid  $^3\text{He}$ , Phys. Rev. B **75**, 174503 (2007); **87**, 019904(E) (2013).
- <sup>20</sup> J. J. Wiman and J. A. Sauls, Strong-Coupling and the Stripe Phase of  $^3\text{He}$ , J. Low Temp. Phys. **184**, 1054 (2016).
- <sup>21</sup> Y. Hasegawa, On Vortex in Superfluid  $^3\text{He-B}$ , Prog. Theor. Phys. **73**, 1258 (1985).
- <sup>22</sup> D. S. Greywall,  $^3\text{He}$  specific heat and thermometry at millikelvin temperatures, Phys. Rev. B **33** 7520 (1986).

<sup>23</sup> E. V. Thuneberg, Hydrostatic Theory of Superfluid  $^3\text{He-B}$ ,  
J. Low Temp. Phys. **122**, 657 (2001).